Effect of lithium fluoride on thermal stability of proton-conducting Ba(Zr0.8-xCexY0.2)O2.9 ceramics

Authors: C.-S. Tu, C.-C. Huang, S.C. Lee, R.R. Chien, V.H. Schmidt, and C.-L. Tsai

C.-S. Tu, C.-C. Huang, S.C. Lee, R.R. Chien, V.H. Schmidt, and C.-L. Tsai, "Effect of lithium fluoride on thermal stability of proton-conducting Ba(Zr0.8-xCexY0.2)O2.9 ceramics," Solid State Ionics 181, 1654-1658 (2010). doi: 10.1016/j.ssi.2010.09.052.

Effect of lithium fluoride on thermal stability of proton-conducting $Ba(Zr_{0.8-x}Ce_xY_{0.2})O_{2.9}$ ceramics

C.-S. Tu [a,*], C.-C. Huang [a], S.C. Lee [a], R.R. Chien [b], V.H. Schmid [b], C.-L. Tsai [b]

[a] Department of Physics, Fu Jen Catholic University, Taipei 242, Taiwan, Republic of China
[b] Department of Physics, Montana State University, Bozeman, MT 59717, USA

A B S T R A C T

In-situ X-ray diffraction (XRD) and micro-Raman scattering have been used to study the thermal stability of lithium fluoride (LiF)-added (7% weight ratio) $Ba(Zr_{0.8-x}Ce_xY_{0.2})O_{2.9}$ (BZCY: $x=0.1$ and 0.2) proton-conducting ceramic powders as a function of temperature in 1 atm of flowing CO_2. This work reveals that LiF-addition can reduce the thermal stability of $Ba(Zr_{0.8-x}Ce_xY_{0.2})O_{2.9}$ in CO_2 and cause decomposition to $BaCO_3$, and possibly $Ba_3Ce_2(CO_3)_5F_2$ (or $CeCO_3F$), and Y_2O_3-like compound after exposure to CO_2 from high temperatures. LiF-related compounds can be removed after calcining (or sintering) in air above 1200 °C, but a minor amount of a Y_2O_3-like compound could remain after calcining at 1400 °C in air.

1. Introduction

One important issue facing proton-conducting ceramics for applications of hydrogen purification and solid oxide fuel cells (SOFCs) is the thermal instability to the environment, especially reaction with coal syngas components such as CO_2 and H_2S [1,2]. However, the effects of coal syngas species on SOFC related materials are not presently well known. Though proton conductors are promising candidates for SOFCs because of their low ionic activation energy [3–6], the major challenge for these materials is to find a proper compromise between ionic conductivity and thermal (or chemical) stability in various environments and operation temperatures (typically 700–850 °C).

$BaCeO_3$ has been known to exhibit high ionic conductivity at high temperatures (≥500 °C) but a poor thermal stability was observed in CO_2 and H_2O atmospheres [3–7]. On the other hand, yttrium-doped $BaZrO_3$ shows a sufficient thermal stability [8,9]. Zr substitution for Ce can improve the thermal stability but decreases the ionic conductivity. Partially substituting Zr for Ce reduces its tendency to decompose into $BaCO_3$ and other oxides in a CO_2-containing environment at intermediate temperatures (700–850 °C). Thus, it has been a goal to find doped $Ba(Zr,Ce)O_3$ ceramics with sufficient ionic conductivity and thermal stability by replacing a fraction of cerium with Zr or other stable dopants.

By thermal gravimetric analysis (TGA) and XRD, $Ba(Ce_{0.9}Y_{0.1})O_{3-\delta}$ (BCY10) powder was confirmed to be kinetically stable below 500 °C and then decomposes completely to $BaCO_3$, CeO_2, and Y_2O_3 after exposure to pure CO_2 at 860 °C [10]. Similarly, XRD results of BCY10 heated in the region of 700–1000 °C in pure CO_2 revealed $BaCO_3$ and fluorite-like CeO_2 structures [11]. It was found that BCY10 can absorb 0.13 g of CO_2 per ceramic gram [11]. $Ba(Ce_{0.9}Nd_{0.1})O_{3-\delta}$ (BCN) ceramic showed decomposition to $BaCO_3$ and CeO_2 in 1 atm CO_2 before reaching 1200 °C, above which the BCN ceramics reacted with alumina or zirconia in the crucible, leading to the loss of barium and an excess of cerium [12]. Differential thermal analysis (DTA) and TGA of Gd- and Nd-doped $Ba(Ce,Zr)O_3$ solid solutions showed a reaction with CO_2 above 600 °C and a reverse reaction near 1150 °C for low Zr content [13].

$Ba(Zr_{0.4}Ce_{0.5})Y_{0.1}O_{3-\delta}$ showed a good thermal stability after exposure to CO_2 at 900 °C [13]. The total ionic conductivity of $Ba(Zr_xCe_{0.9-x}Y_{0.1})O_{3-\delta}$ ($x=0.0$–0.9) in wet H_2 ($pH_2O=1.7\times10^3$ Pa) varies from 3.5×10^{-2} to 3.0×10^{-3} S/cm at 800 °C [14]. The XRD spectra of $Ba(Zr_{0.4}Ce_{0.5}Y_{0.1})O_{2.95}$ and $Ba(Zr_{0.6}Ce_{0.3}Y_{0.1})O_{2.95}$ sintered pellets showed good chemical stability after being boiled in water or after being exposed to CO_2 at 900 °C [15]. In recent stability work, the calcined $Ba(Zr_{0.8-x}Ce_xY_{0.2})O_{3-\delta}$ powders synthesized by the sol–gel method exhibited a good chemical stability for $x<0.3$ after exposure to CO_2 at 900 °C [16]. Similarly, XRD results of $Ba(Zr_{0.8-x}Ce_xY_{0.2})O_{3-\delta}$ powders prepared by the sol–gel process showed a decomposition of $BaCO_3$ for $x\geq0.4$ after treatment in a CO_2 atmosphere at 650 °C [17].

$Ba(Zr_{0.1}Ce_{0.7}Y_{0.2})O_{3-\delta}$ (BZCY172) remained unchanged at 500 °C and exhibited sufficient stability in 2% CO_2 (with H_2) or H_2 (with H_2O) [18]. Conductivities of BZCY172 in humid 4% H_2/Ar are about 9×10^{-3} and 2×10^{-2} S/cm at 500 and 700 °C, respectively [18]. Ba_2

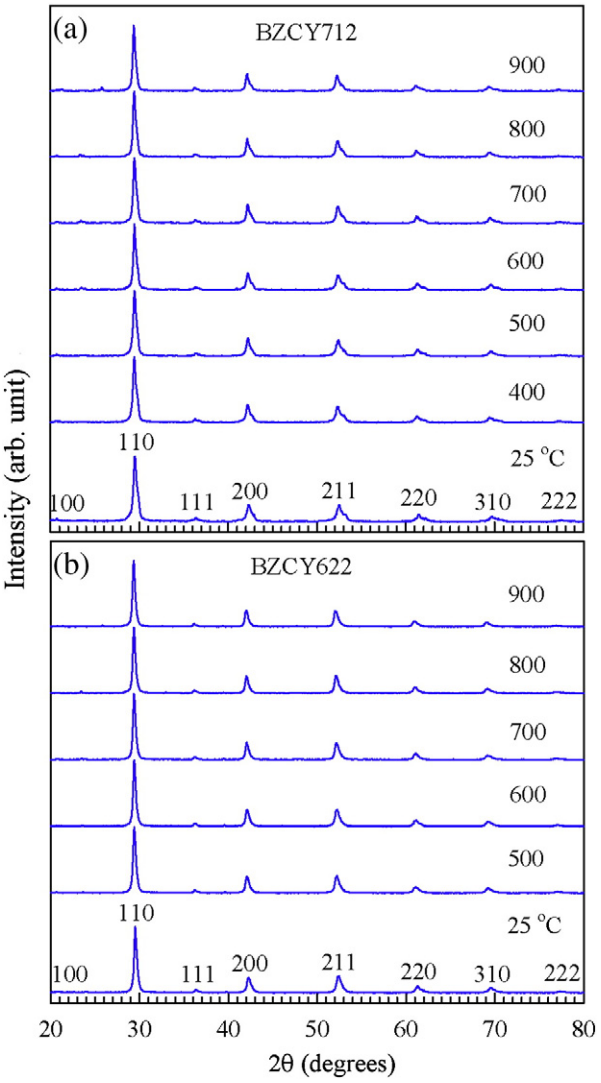

Fig. 1. XRD spectra of calcined (a) BZCY712 and (b) BZCY622 without addition of LiF in 1 atm CO_2 upon heating.

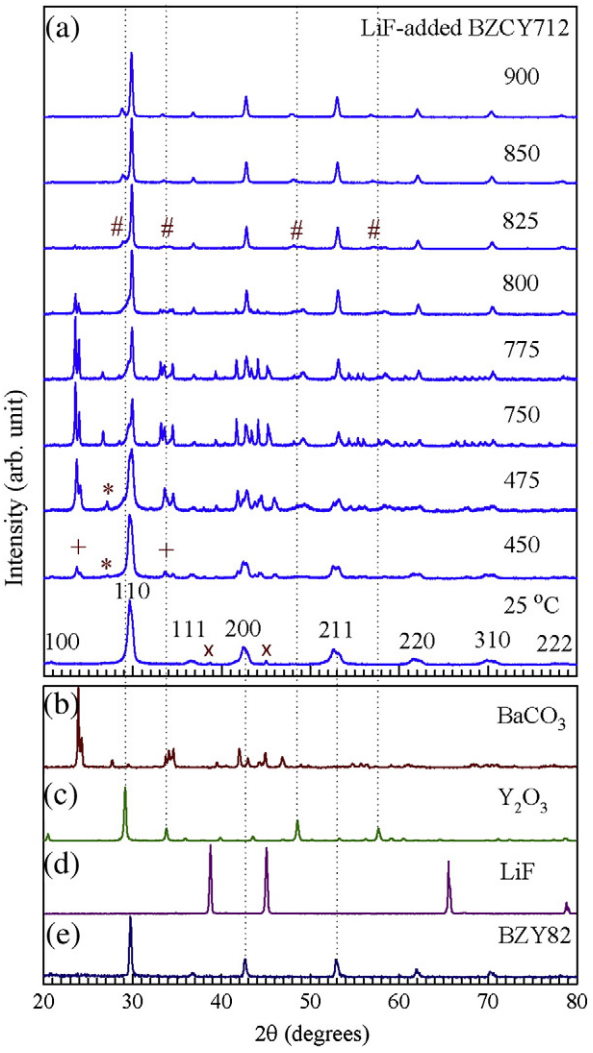

Fig. 2. (a) XRD spectra of 7 wt.% LiF-added BZCY712 in 1 atm CO_2 upon heating. The XRD spectra of (b) $BaCO_3$, (c) Y_2O_3, (d) LiF, and (e) calcined BZY82 powders (without LiF). "+", "*", "#", and "×" indicate $BaCO_3$, possible $Ba_3Ce_2(CO_3)_5F_2$ (or $CeCO_3F$), Y_2O_3-like compound, and LiF, respectively. The dotted lines are guides for eyes.

$(Ca_{0.75}Nb_{0.59}Ta_{0.66})O_{6-\delta}$, $Ba_2(Ca_{0.75}Nb_{0.66}Ta_{0.59})O_{6-\delta}$, and $Ba_2(Ca_{0.79}Nb_{0.66}Ta_{0.55})O_{6-\delta}$ showed long-term stability in boiling water and CO_2 at 800 °C [19]. I*n-situ* XRD and post Raman spectra of Ba$(Zr_{0.6}Ce_{0.2}Y_{0.2})O_{2.9}$ (BZCY622) and Ba$(Zr_{0.8}Y_{0.2})O_{2.9}$ (BZY82) exhibited a sufficient thermal stability in 1 atm CO_2 without obvious decomposition [20]. Conductivities of Ba$(Zr_{0.8-x}Ce_xY_{0.2})O_{2.9}$ synthesized without LiF for $x=0.8$, 0.5, 0.3, and 0.0 in wet H_2 at 700 °C are 1.47×10^{-2}, 1.14×10^{-2}, 7.10×10^{-3}, and 5.68×10^{-3} S/cm, respectively [21].

Lithium fluoride (LiF) has been used as a sintering aid to reduce the sintering temperature and also to enhance density in SOFC ceramics [22]. However, there is not much knowledge on the effects of adding LiF on thermal stability under CO_2 atmosphere. In this work, *in-situ* temperature-dependent XRD and micro-Raman scattering were employed to investigate the effect of 7 wt.% LiF-addition on thermally structural stability of calcined Ba$(Zr_{0.7}Ce_{0.1}Y_{0.2})O_{2.9}$ (BZCY712) and Ba$(Zr_{0.6}Ce_{0.2}Y_{0.2})O_{2.9}$ (BZCY622) powders in 1 atm of flowing CO_2. The post micro-Raman spectra were obtained after exposure to CO_2 at high temperatures.

2. Experimental

Ba$(Zr_{0.8-x}Ce_xY_{0.2})O_{2.9}$ (BZCY: $x=0.1$ and 0.2) ceramic powders were synthesized by the glycine–nitrate process and then were calcined at 1300 °C in laboratory air for 5 h to ensure a single perovskite phase. The 7 wt.% LiF powder was added in calcined BZCY powders before the milling process. After the milling process, the as-prepared LiF-added BZCY solution was dried into powder in an oven. For *in-situ* X-ray diffraction measurements, a high-temperature Rigaku Model MultiFlex X-ray diffractometer was used. In our present experimental results, separate peaks for these two wavelengths could not be resolved. As-prepared LiF-added BZCY ceramic powders were placed and smoothly pressed on the platinum sample holder. The temperature was raised in steps from room temperature in 1 atm of flowing CO_2. Each XRD scan was taken after holding the sample at the setting temperature for about 10 min to ensure a complete reaction with CO_2. In addition, the XRD and micro-Raman spectra were measured after subsequent exposure to CO_2 at 850 °C for previously calcined (at 1200 °C in air for 5 h) 7 wt.% LiF-added BZCY powders. The post XRD and micro-Raman spectra were also obtained for 7 wt.% LiF-added BZCY after calcining in air at 1400 °C for 5 h.

A double grating Jobin Yvon Model U-1000 double monochromator with 1800 grooves/mm gratings and a nitrogen-cooled CCD as a detector were employed for micro-Raman scattering. A Coherent Model Innova 90 argon laser with $\lambda=514.5$ nm was used as an excitation source.

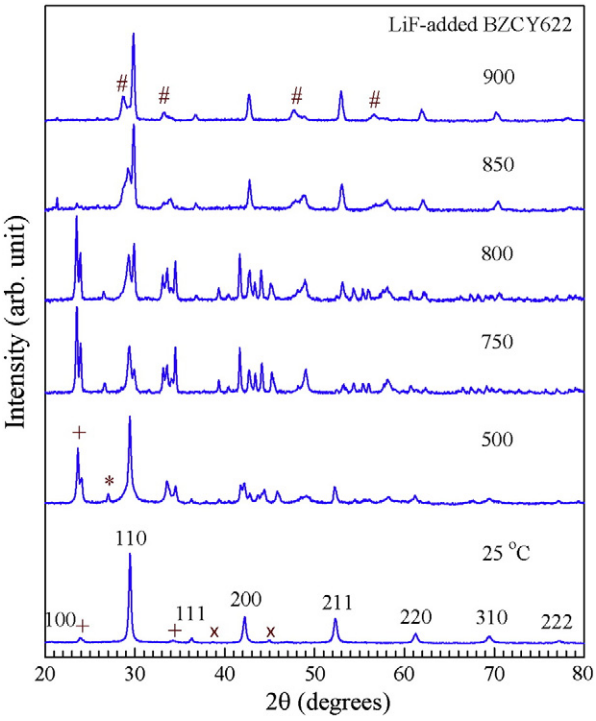

Fig. 3. XRD spectra of LiF-added BZCY622 upon heating in 1 atm CO_2. "+", "*", "#", and "×" indicate $BaCO_3$, possibly $Ba_3Ce_2(CO_3)_5F_2$ (or $CeCO_3F$), Y_2O_3-like compound, and LiF, respectively.

3. Results and discussion

Fig. 1 shows the temperature-dependent XRD spectra of calcined $Ba(Zr_{0.7}Ce_{0.1}Y_{0.2})O_{2.9}$ (BZCY712) and $Ba(Zr_{0.6}Ce_{0.2}Y_{0.2})O_{2.9}$ (BZCY622) ceramic powders without addition of LiF in 1 atm of flowing CO_2 from 25 to 900 °C. The calcined BZCY712 and BZCY622 powders exhibit a good thermal stability in CO_2 without apparent second phase or chemical decomposition upon heating. The main diffraction peaks of calcined BZCY712 and BZCY622 powders include (100), (110), (111), (200), (211), (220), (310), and (222), suggesting a simple-cubic perovskite structure [23].

Figs. 2(a) and 3 shows the temperature-dependent XRD spectra of as-prepared LiF-added $Ba(Zr_{0.7}Ce_{0.1}Y_{0.2})O_{2.9}$ (BZCY712) and $Ba(Zr_{0.6}Ce_{0.2}Y_{0.2})O_{2.9}$ (BZCY622) powders in 1 atm of flowing CO_2 upon heating. To identify possible chemical decomposition, the XRD spectra of $BaCO_3$, Y_2O_3, and LiF powders were obtained at room temperature as shown in Fig. 2(b)–(d). The main diffraction peaks of as-prepared LiF-added BZCY712 and BZCY622 powders at 25 °C include (100), (110), (111), (200), (211), (220), (310), and (222), suggesting a simple-cubic perovskite structure [23]. The cubic lattice parameters (a) at 25 °C are 4.258 Å and 4.286 Å respectively for LiF-added BZCY712 and BZCY622 powders estimated from the (110) peaks ($2\theta = 29.65°$ and 29.45°). With estimated values from (200) and (211) reflections, the standard deviation is about 0.004 Å for both BZCY712 and BZCY622 powders. The lattice parameter of BZCY622 is slightly greater than that of BZCY712 because the radius of Ce^{4+} ($R^{VI} = 0.87$ Å) is larger than for Zr^{4+} ($R^{VI} = 0.72$ Å) [24]. A minor broad shoulder seen in the high-2θ XRD peaks of BZCY712 possibly associates with BZY82, whose XRD spectrum is given in Fig. 2(e). The dotted lines indicate the structural correlation between BZCY712 and BZY82 at room temperature.

Upon heating in 1 atm of flowing CO_2, the XRD spectra remain almost the same below 450 °C without obvious decomposition. However, above 450 °C several decomposition peaks appear in LiF-added BZCY712 and BZCY622 [Figs. 2(a) and 3] as denoted by "+" and "*", indicating $BaCO_3$ and possibly $Ba_3Ce_2(CO_3)_5F_2$ (or $CeCO_3F$).

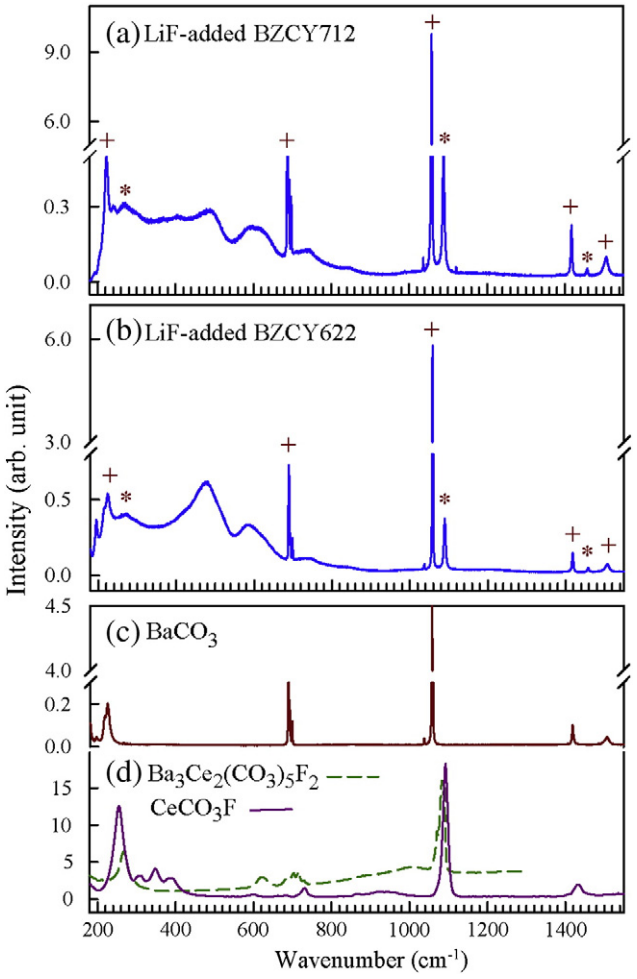

Fig. 4. Post Raman spectra of LiF-added (a) BZCY712, (b) BZCY622 after exposure to 1 atm CO_2 from 900 °C, (c) $BaCO_3$, and (d) $Ba_3Ce_2(CO_3)_5F_2$ and $Ce(CO_3)F$. "+" and "*" indicate $BaCO_3$ and possibly $Ba_3Ce_2(CO_3)_5F_2$ [or $Ce(CO_3)F$]. [Raman spectra of $Ba_3Ce_2(CO_3)_5F_2$ and $Ce(CO_3)F$ are cited from the database at http://rruff.info/.]

The identification of $Ba_3Ce_2(CO_3)_5F_2$ (or $CeCO_3F$) is mainly based on Raman spectra given in Fig. 4(d). As the temperature increases, the relative intensities of "+" and "*" peaks grow gradually up to 775 °C and then vanish essentially above 800 °C. Several minor XRD peaks as indicated by "#" begin to smear out near 800 °C upon heating. Those peaks likely correspond to the Y_2O_3-like structure as compared with the XRD peaks of Y_2O_3 in Fig. 2(c).

Fig. 4(a) and (b) shows the post Raman spectra of LiF-added BZCY712 and BZCY622 powders after exposure to 1 atm of flowing CO_2 from 900 °C. To identify possible chemical decomposition, the Raman spectra of $BaCO_3$, $Ba_3Ce_2(CO_3)_5F_2$ and $CeCO_3F$ are given in Fig. 4(c) and (d). The main vibrations of $BaCO_3$ include 225, 690, 1059, and 1419 cm^{-1}. The CO_3^{2-} ion (D_{3h} symmetry) has four normal vibration modes: $A_1'(R) + A_2''(IR) + E'(R, IR) + E''(R, IR)$ [25]. "R" and "IR" indicate the Raman and infrared active modes, respectively. The 690, 1059, and 1419 cm^{-1} vibrations respectively correspond to the doubly degenerate bending vibration (E''), symmetric stretching vibration (A_1'), and doubly degenerate asymmetric stretching vibration (E') of the CO_3^{2-} ion.

As given in Fig. 4(d), $Ba_3Ce_2(CO_3)_5F_2$ and $CeCO_3F$ have two similar major Raman vibrations of 267 and 1084, and 254 and 1093 cm^{-1}, respectively. Raman vibrations of 690, 1059, and 1419 cm^{-1} of $BaCO_3$ appear in LiF-added BZCY712 and BZCY622 after exposure to 1 atm CO_2 from 900 °C as indicated by "+" in Fig. 4(a) and (b). In addition, 270 and 1090 cm^{-1} vibrations of possibly $Ba_3Ce_2(CO_3)_5F_2$ (or $CeCO_3F$) as indicated by "*" were also observed in LiF-added BZCY712 and BZCY622.

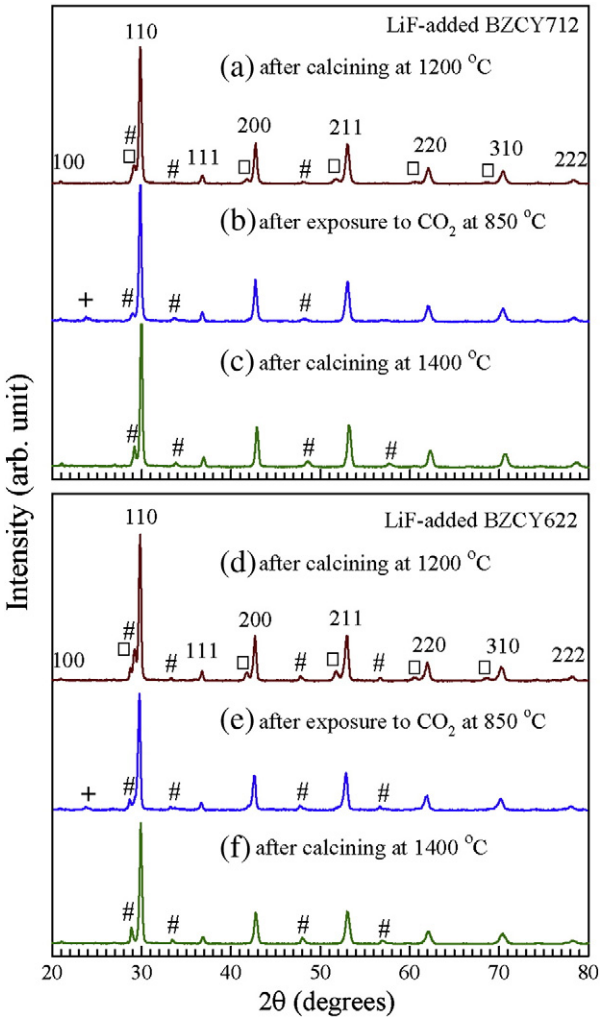

Fig. 5. Post XRD spectra of LiF-added BZCY712 and BZCY622 (a and d) after calcining at 1200 °C in air for 5 h, (b and e) after subsequent exposure to CO_2 at 850 °C for previously calcined powders at 1200 °C for 5 h, and (c and f) after calcining at 1400 °C in air for 5 h. "+" and "#" indicate $BaCO_3$ and Y_2O_3-like structure, respectively. "□" represents possibly high-cerium BZCY.

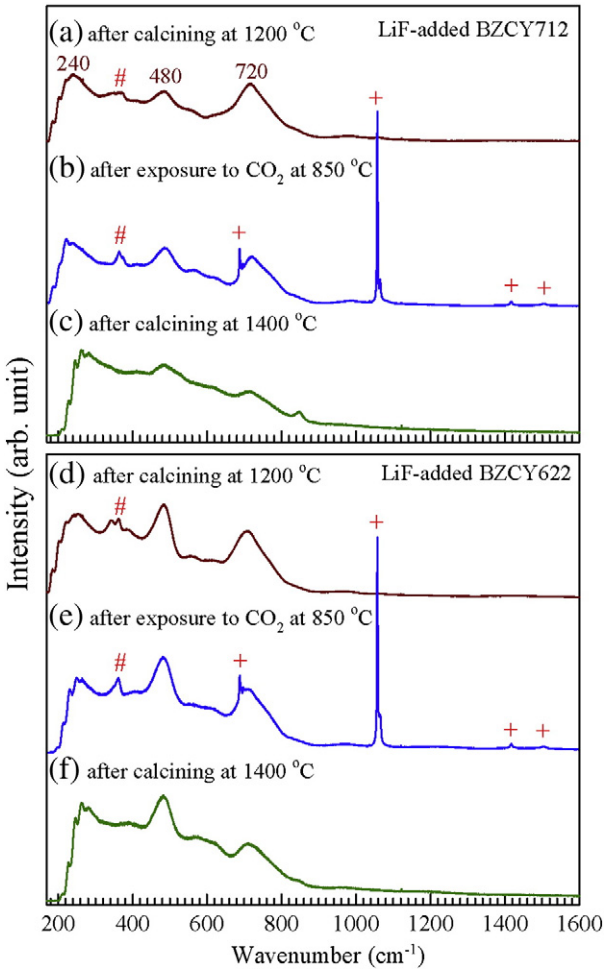

Fig. 6. Post Raman spectra of LiF-added BZCY712 and BZCY622 (a and d) after calcining at 1200 °C for 5 h, (b and e) after subsequent exposure to CO_2 at 850 °C for previously calcined powders at 1200 °C for 5 h, and (c and f) after calcining at 1400 °C in air for 5 h. "+" and "#" indicate Raman modes of $BaCO_3$ and Y_2O_3-like structure.

To study the effect of the calcining temperature, Fig. 5(a) and (d) show the post XRD spectra of LiF-added BZCY712 and BZCY622 powders after calcining at 1200 °C in laboratory air for 5 h. "#" and "□" indicate Y_2O_3-like structure and possibly high-cerium BZCY, respectively. $BaCO_3$ and possibly $Ba_3Ce_2(CO_3)_5F_2$ (or $CeCO_3F$) do not occur after calcining in air at 1200 °C and also were not observed in the post Raman spectra as shown in Fig. 6(a) and (d).

Fig. 5(b) and (e) are the post XRD spectra after subsequent exposure to CO_2 at 850 °C for previously calcined (at 1200 °C for 5 h) LiF-added BZCY712 and BZCY622 powders. The $BaCO_3$ was observed in both BZCY712 and BZCY622 as indicated by "+". The Raman modes of $BaCO_3$ were confirmed by vibrations of 690, 1059, and 1419 cm^{-1} as seen in Fig. 6(b) and (e). In addition, the Raman mode near 370 cm^{-1} which likely associates with the major vibration 375 cm^{-1} of Y_2O_3 [20], was observed in LiF-added BZCY712 and BZCY622 after subsequent exposure to CO_2 at 850 °C as shown in Fig. 6 (b) and (e). This is consistent with the Y_2O_3-like structure as indicated by "#" in Figs. 5 and 6.

As seen in Fig. 5(a, b, d, and e), the high-cerium XRD peaks shown by "□" appear after calcining in air at 1200 °C, but then disappear after subsequent exposure to 1 atm CO_2 at 850 °C. This disappearance results from the CO_2 reacting much more strongly with the high-cerium material compared to the original BZCY712 or BZCY622. In addition, the $BaCO_3$ peaks shown by "+" after the 850 °C exposure to CO_2 result mostly from the loss of Ba from the high-cerium BZCY.

Fig. 5(c) and (f) show the post XRD spectra of LiF-added BZCY712 and BZCY622 powders after calcining at 1400 °C in air for 5 h. The $BaCO_3$ and possibly $Ba_3Ce_2(CO_3)_5F_2$ (or $CeCO_3F$) structures are not observed as confirmed in the Raman spectra of Fig. 6(c) and (f). The possibly high-cerium BZCY compound (as indicated by "□" in Fig. 5) is not observed, but the Y_2O_3-like compound still remains in the powders after calcining at 1400 °C. These results suggest that LiF-related compounds can be removed after calcining (or sintering) above 1200 °C, but chemical decomposition (such as Y_2O_3-like compound) can be induced.

Comparing Fig. 6(a) and (c) for LiF-added BZCY712, and Fig. 6(d) and (f) for LiF-added BZCY622, the major Raman peaks appear near 240, 480, and 720 cm^{-1} in both compounds after calcining at 1200 and 1400 °C. Note that the major vibrations of CeO_2 and ZrO_2 are 461 and 474 cm^{-1}, respectively [26,27]. The 474 cm^{-1} vibration of ZrO_2 corresponds to the O–O vibration of the A_g mode [26]. The 461 cm^{-1} of CeO_2 corresponds to the F_{2g} Raman-active mode of the fluorite structure [27]. Thus, the 480 cm^{-1} peak likely associates with the O–O vibration in the BZCY perovskite structure.

In the recent study by Tsai et al. [22], nuclear reaction analysis (which is sensitive to elemental concentration) showed negligible residue of Li in 7 wt.% LiF-added BZCY622 solid ceramic after sintering at 1400 °C for various dwell times [22]. The 7 wt.% LiF-addition does not reduce conductivity, but rather slightly improves the total

conductivity of BZCY ($x = 0.0$–0.4) ceramics measured at 700 °C in a water saturated 4% H_2 + 96% Ar atmosphere [22].

4. Conclusions

In-situ temperature-dependent XRD and Raman scattering spectra in 1 atm of flowing CO_2 reveal that 7 wt.% LiF-addition in BZCY712 and BZCY622 ceramic powders can cause chemical decomposition to $BaCO_3$, possibly $Ba_3Ce_2(CO_3)_5F_2$ (or $CeCO_3F$), Y_2O_3-like compound, and high-cerium BZCY. The LiF can react with BZCY712 and BZCY622 powders above ~450 °C in CO_2 upon heating and then significantly causes decomposition and structural instability. After calcining at 1200 or 1400 °C for 5 h, fluorine-related compounds, such as $Ba_3Ce_2(CO_3)_5F_2$ (or $CeCO_3F$), do not appear after subsequent exposure to CO_2 at 850 °C. The post XRD and Raman spectra of LiF-added BZCY712 and BZCY622 powders after calcining at 1200 or 1400 °C for 5 h, do not show existence of $Ba_3Ce_2(CO_3)_5F_2$ (or $CeCO_3F$). LiF-related compounds can be removed after calcining at high temperatures ($\geq$1200 °C), but a minor decomposition to the Y_2O_3-like compound could be induced. The degree of the LiF-addition effect on phase thermal stability and electrochemical properties likely depends on the working environment, especially under high-concentration CO_2 atmosphere.

Acknowledgements

The authors would like to thank Dr. J. Liang for the micro-Raman scattering apparatus. This work was supported by DOE under subcontract DEAC06-76RL01830 from Battelle Memorial Institute and PNNL.

References

[1] J.P. Trembly, R.S. Gemmen, D.J. Bayless, J. Power Sources 163 (2007) 986.
[2] R.S. Gemmen, J. Trembly, J. Power Sources 161 (2006) 1084.
[3] S. Mclntosh, R.J. Gorte, Chem. Rev. 104 (2004) 4845.
[4] S.M. Haile, Acta Mater. 51 (2003) 5981.
[5] C.W. Tanner, A.V. Virkar, J. Electrochem. Soc. 143 (1996) 1386.
[6] S.V. Bhide, A.V. Virkar, J. Electrochem. Soc. 146 (1999) 2038.
[7] G. Ma, T. Shimura, H. Iwahara, Solid State Ionics 110 (1998) 103.
[8] F.M.M. Snijkers, A. Buekenhoudt, J. Cooymans, J.J. Luyten, Scr. Mater. 50 (2004) 655.
[9] A. Magrez, T. Schober, Solid State Ionics 175 (2004) 585.
[10] N. Zakowsky, S. Williamson, J.T.S. Irvine, Solid State Ionics 176 (2005) 3019.
[11] B.R. Sneha, V. Thangadurai, J. Solid State Chem. 180 (2007) 2661.
[12] F. Chen, O.T. Sorensen, G. Meng, D. Peng, J. Mater. Chem. 7 (1997) 481.
[13] K.H. Ryu, S.M. Haile, Solid State Ionics 125 (1999) 355.
[14] K. Katahira, Y. Kohchi, T. Shimura, H. Iwahara, Solid State Ionics 138 (2000) 91.
[15] Z. Zhong, Solid State Ionics 178 (2007) 213.
[16] E. Fabbri, A. D'Epifanio, E.D. Bartolomeo, S. Licoccia, E. Traversa, Solid State Ionics 179 (2008) 558.
[17] Y. Guo, Y. Lin, R. Ran, Z. Shao, J. Power Sources 193 (2009) 400.
[18] C. Zuo, S. Zha, M. Liu, M. Hatano, M. Uchiyama, Adv. Mater. 18 (2006) 3318.
[19] S.S. Bhella, V. Thangadurai, J. Power Sources 186 (2009) 311.
[20] C.-S. Tu, R.R. Chien, V.H. Schmidt, S.-C. Lee, C.-C. Huang, C.-L. Tsai, J. Appl. Phys. 105 (1-7) (2009) 103504.
[21] E. Fabbri, A. D'Epifanio, E.D. Bartolomeo, S. Licoccia, E. Traversa, Solid State Ionics 179 (2008) 558.
[22] C.-L. Tsai, M. Kopczyk, R.J. Smith, V.H. Schmidt, Solid State Ionics 181 (2010) 1083–1090.
[23] B.D. Cullity, Elements of X-ray Diffraction, Addison-Wesley Publishing, 1978.
[24] R.D. Shannon, Acta Crystallogr. A32 (1976) 751.
[25] R.L. Frost, J.M. Bouzaid, J. Raman Spectrosc. 38 (2007) 873.
[26] B.-K. Kim, H.-O. Hamaguchi, Phys. Status Solidi B 203 (1997) 557.
[27] R.Q. Long, Y.P. Huang, H.L. Wan, J. Raman Spectrosc. 28 (1997) 29.